Lasers in Manufacturing and Materials Processing (2024) 11:109–124
https://doi.org/10.1007/s40516-023-00233-6

RESEARCH

Studies on the Use of Laser Directed Energy Deposition for the Additive Manufacturing of Lightweight Parts

Avelino Zapata[1] · Christian Bernauer[1] · Matous Celba[2] · Michael F. Zaeh[1]

Accepted: 30 November 2023 / Published online: 8 December 2023

Abstract

Despite the numerous benefits of battery electric vehicles, their relatively short maximal range compared to internal combustion engine vehicles limits their attractiveness to the consumer. Implementing lightweight structures is one solution to reduce the mass of the vehicle, which in turn lowers the energy consumption and thus extends the maximal range. Additive Manufacturing processes, such as the Laser Directed Energy Deposition (DED-LB), offer great potential for the resource-efficient manufacturing of lightweight components because they allow producing near-net-shaped parts of variable sizes and geometries. Therefore, in this study, DED-LB was assessed concerning its use for the rapid manufacturing or modification of lightweight parts. The additive process was performed on EN AW 6060 aluminum extrusion profiles commonly found in battery electric vehicles and an AlSi10Mg wire was used as feedstock. The investigations included temperature and microhardness measurements. Furthermore, the effect of the deposition rate on the geometric quality of the part was investigated. The results indicate that DED-LB can be performed on thin-walled structures to produce defect-free components. Furthermore, the findings reveal a trade-off between a fast build-up and the surface quality of the parts. Notably, it was observed that the different deposition rates had no impact on the hardness of the produced parts. Further studies on heat management are needed to optimize the process for producing lightweight parts with improved mechanical properties.

Keywords Lightweight structures · Resource-efficient production · Annular laser spot · Laser Directed Energy Deposition · Rapid manufacturing

✉ Avelino Zapata
avelino.zapata@iwb.tum.de

[1] TUM School of Engineering and Design, Department of Mechanical Engineering, Institute for Machine Tools and Industrial Management, Technical University of Munich, Boltzmannstr. 15, 85748 Garching, Germany

[2] Faculty of Mechanical Engineering, Czech Technical University in Prague, Technická 4, Prague 16607, Czech Republic

Introduction

Electric vehicles have contributed to effectively reduce traffic-induced pollution, caused by the emission of greenhouse gases [1]. Nevertheless, the limited range of electric vehicles, when compared to combustion engine vehicles, remains a major challenge that needs to be overcome to improve their attractiveness for consumers [2]. Simply scaling up the battery size is not a viable solution as it would further increase the mass of the vehicle, which in turn negatively affects its acceleration, rolling, and climbing resistances [3]. Therefore, mass-related efficiency trade-offs must be considered when dimensioning the battery [4]. One solution to reduce the total vehicle mass without reducing the battery size is the implementation of lightweight structures [5]. Additive Manufacturing (AM) processes show a great potential for the efficient manufacturing of lightweight components, as they allow manufacturing parts with variable and complex geometries in a single system [6]. In AM technologies, three-dimensional (3D) parts are manufactured by progressively adding layers of material on a substrate. Powder bed fusion (PBF) processes are among the most discussed AM technologies for manufacturing highly complex parts in the automotive field [7]. In PBF, the build platform is covered with a thin layer of powder, and the two-dimensional contour of the part is molten selectively within the confined area by a laser beam (LB). Thereafter, the build platform is lowered, a new layer of powder is applied, and the melting process is restarted. This procedure results in relatively slow build rates and substantial limitations with regard to the maximal size of the manufactured components, thus limiting possible applications [8].

Directed Energy Deposition (DED) processes are well-suited AM processes to manufacture large parts, as the feedstock only needs to be supplied locally into a moving melt pool. The maximal size of the parts that can be manufactured with these technologies is thereby only limited by the range of motion of the kinematic system. The feedstock can be delivered in the form of powder or wire. A wire as feedstock offers several benefits, including easier handling, higher material utilization, higher deposition rates, and increased operational safety [9, 10]. Various energy sources can be installed to induce the melt pool. The electric arc is a widespread method due to the high availability and reasonable price of the systems commonly used for welding. However, methods that use a laser beam or an electron beam provide a more concentrated energy input and are therefore better suited for producing near-net-shape components [11]. For the Laser Directed Energy Deposition (DED-LB) process with wire as feedstock, the wire must be fed coaxially to the laser beam to obtain a direction-independent process [12]. Two solutions have been developed to achieve the coaxial alignment of the supplied feedstock and the laser beam. Either multiple laser beams are focused on the process zone [13] or a hollow laser beam with a ring-shaped profile is formed through optical elements [14, 15]. Both arrangements aim to distribute the intensity as uniformly as possible around the wire so that the process conditions remain the same regardless of the direction of movement. This results in a higher stability and robustness of the process compared to the process variants with lateral wire feeding [16].

The research on enabling new processes to produce parts using lightweight materials, such as aluminum alloys, is essential as they play a crucial role in mass-optimized structures [17, 18]. It has been shown that various aluminum alloys can be processed successfully with DED processes despite the numerous well-known material-specific challenges, such as a high thermal conductivity, a high reflectivity, and a low viscosity [19]. A more frequently used material for AM and casting is AlSi10Mg. The hardness of the parts produced with this material using DED [20, 21] or PBF [22] is comparable to the hardness of parts produced by casting [23, 24]. Another commonly used aluminum alloy in the automotive industry is EN AW 6060, especially for extrusion profiles. Studies conducted by Kronthaler et al. [25] have shown that although it is challenging, it is possible to weld parts made of this alloy without leading to bead defects, such as pores, using laser technologies. With the idea of producing hybrid structures, Nahmany et al. [26] and Shribman et al. [27] studied the properties of a joint between additively manufactured AlSi10Mg parts and EN AW 6060. The results of both studies indicate the possibility of manufacturing hybrid structures featuring no visible defects. At the boundary section, these structures exhibit a hardness equivalent to the average of both base materials.

In recent years, researchers have begun to explore using DED-LB with aluminum alloys as feedstock for the automotive sector. These processes offer a unique advantage by allowing the additive modification of premanufactured parts, which enables a more flexible and resource-efficient production [28]. As a result, hybrid parts can be manufactured by adding features or coatings to the components [29], and damaged parts can be repaired [30]. DED-LB also allows for the geometrical customization of semi-finished components, thus eliminating the need for a complete part redesign and remanufacturing [7]. In this context, Bruzzo et al. [31] suggested a new design paradigm based on manufacturing value-adding functional features on low-cost base parts, emphasizing the potential of this hybrid production approach to minimize material costs by using the right material in the right place. However, some challenges must be overcome before the DED-LB process can be reliably used for manufacturing hybrid parts. Hagenlocher et al. [32] addressed the heat accumulation in the produced part caused by the periodic heat input and proposed theoretical models that help to correlate the thermal history of a part to the resulting grain structure. Froend et al. [33] further demonstrated that by changing the laser beam irradiances, the cooling rates were influenced and thus led to different microstructures in the part. Kiani et al. [34] focused on finding suitable process parameters for manufacturing single beads, thin walls, and solid blocks, indicating that the parameters suitable for producing thin walls can be transferred to manufacture structures with more volume. The geometrical accuracy of the parts was addressed by Becker et al. [35] and Moehring et al. [36], who implemented closed-loop control of the height by adapting the wire speed and the laser power based on the layer number, resulting in parts with more regular thickness. Finally, the deposition rates that can be accomplished with the DED-LB process were studied by Madarieta et al. [37], who successfully built solid blocks at a deposition rate of 0.7 kg/h using an AL-5356 wire.

The review of the relevant literature reveals that the DED-LB process has great potential for the rapid manufacturing of fully additive as well as hybrid parts.

Both variants contribute to build lightweight structures, which become increasingly important to compensate for the heavy battery storage units in electric vehicles. DED-LB stands out among other AM processes because it allows manufacturing parts of different sizes with high geometrical accuracy on substrates of variable shapes at high build-up rates. Also, based on the results of works that processed aluminum alloys using this technology, it was shown that the produced parts have similar mechanical properties to those produced with established processes, such as casting. The rapidly increasing number of publications in recent years, especially when using wire as feedstock, indicates the interest of both the industry and the research institutions to develop this technology further [38]. However, so far, the use of DED-LB in the industry for manufacturing hybrid parts is scarce, partly due to the lack of studies that address crucial aspects such as the influence of the deposition rate and the process strategy on the quality of the parts. Most of the existing studies were conducted on dispensable substrates, thus not providing insights into the result of the process when performed on thin-walled components.

Therefore, in this work, the DED-LB process with wire (DED-LB-W) was performed on premanufactured extrusion profiles to study the geometrical and mechanical properties of the additive section of the hybrid component. The samples were produced using two different wire speeds to address the influence of the deposition rate, a crucial factor for the industrial use of the process [8]. In the experiments, different interlayer waiting periods were tested. During the manufacturing process, the temperature was measured to correlate the process parameters with the resulting properties of the part. The geometry of the produced thin-walled samples was then analyzed based on the cross-sectional width of the walls and the waviness of the surface. Next, the mechanical properties were studied by performing hardness measurements on cross-sections of the parts. The results show that by using the DED-LB-W process, thin-walled parts could be manufactured at high deposition rates with a constant width and a hardness comparable to parts produced by casting. Furthermore, the results indicate that an optimization for either a rapid build-up or a high-quality surface is possible through the process design. Additionally, the process design allows influencing the hardness of the part, thus allowing a fine-tuning of the mechanical properties. Therefore, this study paves the way for future studies focused on producing highly customized lightweight components.

Experimental

Materials

Extrusion profiles of the aluminum alloy EN AW 6060 were used as the substrates in all experiments. The wall thickness of the substrates was 3 mm. Before the experiments, the profiles were sandblasted and cleaned with isopropanol to obtain reproducible surface conditions. As feedstock material, a standard aluminum alloy wire AlSi10Mg with a diameter of 1.2 mm was used.

Systems

The system setup is displayed in Fig. 1. The DED-LB-W process was conducted using a coaxial deposition head (CoaxPrinter, Precitec GmbH & Co. KG, Germany), which reshaped the incoming laser beam through a combination of axicons to achieve a hollow laser beam resulting in an annular beam profile. This configuration allows to coaxially feed the wire through the hollow laser beam into the melt pool, thus it enables direction-independent process conditions. The laser radiation was generated by a 4 kW disk laser (TruDisk 4001, TRUMPF GmbH & Co. KG, Germany) emitting at a wavelength of 1030 nm in continuous wave mode. The laser beam was transmitted to the deposition head via a light cable with a fiber core diameter of 600 µm. Two copper nozzles were attached to the deposition head and pointed toward the process zone to provide the shielding gas from two opposed directions. The wire was propelled by an industrial wire feeding system produced by the Dinse GmbH (Germany) consisting of a front drive (FD101 LS-WB-K), a slave drive (WD 300 FD), and a control unit (FDE-EC150 HW). To compensate for the curvature of the wire, a two-plane wire straightening unit (DIX DRE 360, Dinse GmbH, Germany) was coupled to the front drive and adjusted as needed. Two kinematic systems were actuated by a robotic control system (KR C4, KUKA AG, Germany). They consisted of a six-axis industrial robot (KR 60, KUKA AG, Germany) with a maximal load capacity of 60 kg and a static positioning repeatability of ± 0.1 mm, which manipulated the deposition head, and a two-axis positioning system (DKP 400, KUKA AG, Germany), on which a cooling plate with inner water circulation was mounted.

The temperature was measured using type K thermocouples with a probe diameter of 0.5 mm and a probe length of 250 mm. The maximum error is specified as ± 2.2 °C or 0.75%, whichever is higher for the measured temperature. A thermal paste was applied to the measurement points to ensure reproducible heat conduction conditions. An optical profilometer (VR 3100, Keyence Corporation, Japan) with a measurement accuracy of ± 3 µm in height and ± 5 µm in length and width was used

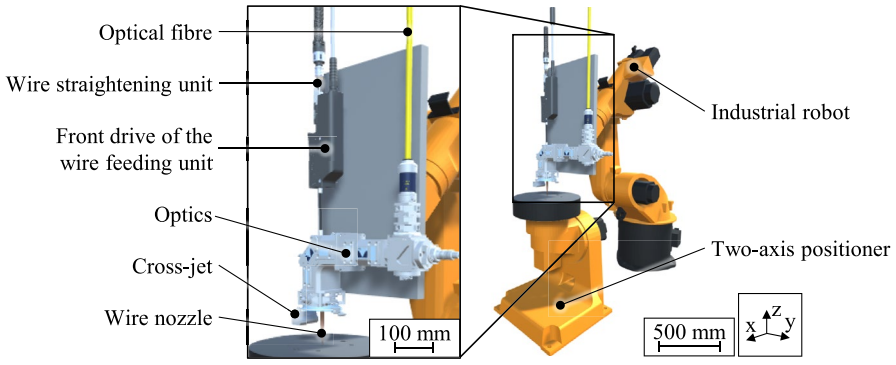

Fig. 1 Digital rendering of the system used in the experiments with a close-up on the main components for the Laser Directed Energy Deposition process with wire

for the three-dimensional (3D) scanning of the surface topography via the light-section method as well as for capturing images of the cross-sections of the samples. The measurement was subsequently carried out using the software of the device (MultiFileAnalyzer version 2.2.093, Keyence Corporation, Japan). Lastly, the hardness measurements were performed with a fully automated hardness tester (Qness 60 A + EVO, ATM Qness GmbH, Germany). The diagonal lengths of the indentations were determined manually in the software to ensure a maximal accuracy [39].

Experimental Procedure

The single-run experimental design is summarized in Table 1. The process parameters were chosen according to the process window identified in a previous study [40]. To investigate the influence of the deposition rate on the geometrical and mechanical properties of the produced parts, experiments with wire speeds of 4 m/min and 8 m/min were performed. Additionally, the interlayer waiting period t_{wait} after the deposition of each layer was varied in the levels of 0 s, 15 s, 30 s, and 60 s. The twenty-layer parts were manufactured using a fixed laser power P_L of 3700 W and a traverse speed v_W of 2 m/min. During the process, the two copper nozzles delivered a total shielding gas flow of 30 l/min.

The manufactured test samples are visualized in Fig. 2a) and the exact measurement positions and dimensions are specified in Fig. 2b). The trajectory of the process corresponded to a squared geometry with a side length of 60 mm and the starting point was placed in the center of one side. The deposition of each consecutive layer started at the same side. The height adjustment per layer was chosen as 0.55 mm for the experiments with a v_W of 4 m/min and 1.1 mm for the experiments with a v_W of 8 m/min. During the process, the temperature was measured at a sampling rate of 2 Hz using three thermocouples. The thermocouples were placed in small, superficial indents at the indicated positions on the interior side of the extrusion profiles since the highest heat accumulation was expected in this section of the part. For the analysis, a mean value for each time step was calculated based on the three recorded time series. To compare the resulting temperature histories for all the different parameter sets, the maximal temperature T_{max} and the initial temperature T_{ini} were determined for each layer. The initial temperature corresponds to the measured temperature just before the next layer is applied, thus being the lowest temperature at each layer.

Table 1 Summary of the parameter sets used in the experiments

Varied parameters	Levels
Wire speed v_W in m/min	4, 8
Interlayer waiting period in s	0, 15, 30, 60
Fixed parameters	Value
Laser power P_L in W	3700
Traverse speed v_T in m/min	2
Number of layers	20

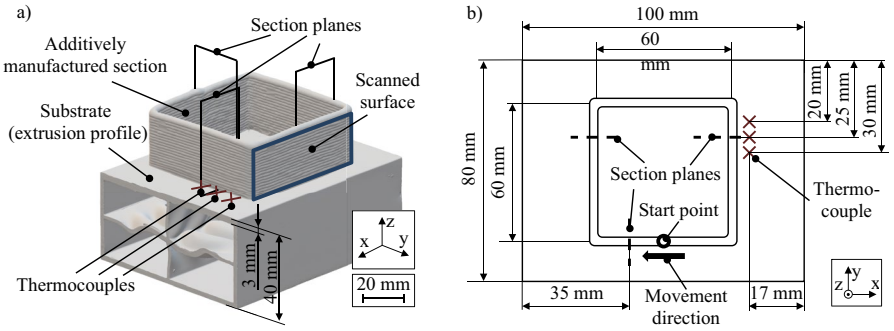

Fig. 2 Schematic visualization of the test specimens: **a** a three-dimensional view and (**b**) top view with the corresponding dimensions and measurement locations

After the experiments, one surface of the additive section of each of the produced parts was scanned to determine the surface waviness. The waviness profiles were acquired using the profilometer based on five vertical lines. A similar method was used by Baier et al. [41]. The location and the dimensions of the lines are shown in Fig. 3a). Next, the maximal height w_z and the arithmetic mean of the line profiles w_a (see DIN EN ISO 25175-2) were taken. An EN ISO 11,562 profile filter with a cutoff wavelength of c = 0.25 mm was applied to the surface profile in order to separate the waviness from the roughness. Furthermore, the samples were cut at three locations (see Fig. 2a)) to obtain cross-sections of the parts. The extracted samples were embedded in resin, ground in three steps (300, 800, and 1200 grit),

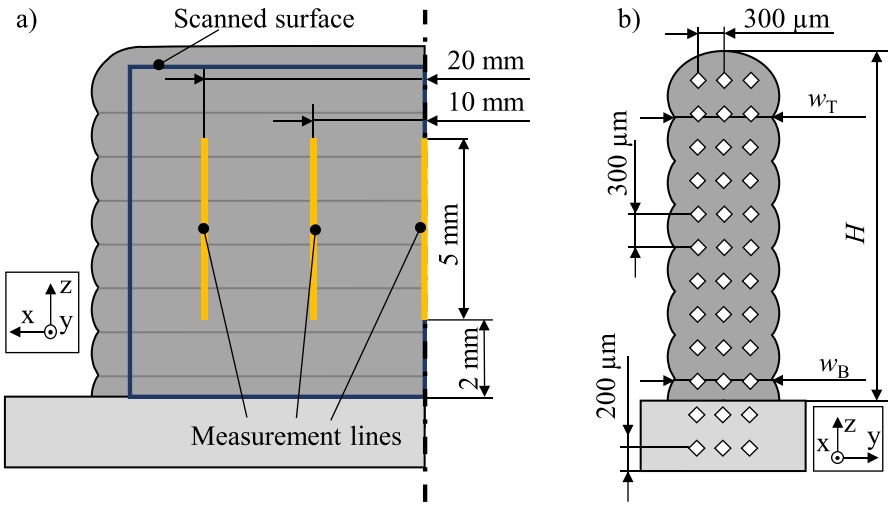

Fig. 3 Measurement configurations: **a** surface measurement to quantify the waviness and (**b**) cross-sectional measurements for determining the dimensions of the part and measuring the hardness, with the measured width at the top w_T and bottom w_B as well as the height H

and then polished in two stages (3 µm and 1 µm). The hardness measurements were conducted following the standard DIN EN ISO 6507-1 and only on the samples extracted close to the position of the temperature measurement. According to this norm, the minimal distance between the center point of two adjacent indentations for lightweight alloys must be six diagonal lengths d of the indentations and three times d away from the edge of the sample. The norm also suggests choosing a test force that results in indentations with a diagonal length larger than 20 µm. Based on preliminary tests, an indentation time of 10 s and a test force of 0.4903 N, corresponding to $HV_{0.05}$, were chosen. This resulted in indentations with a length of 30 µm in the substrate and 40 µm in the additive section. Therefore, a distance of 300 µm was chosen between the indents and the distance toward the edges of the sample was 200 µm, as indicated in Fig. 3b). Next, again using the profilometer and the included software, images of the cross-sections were taken to measure the width of the wall at the bottom w_B and at the top w_T, as well as the height of the wall H. The value w_B was measured at the narrowest section between the first and the second layer and the value w_T at the narrowest section between the last two layers (see Fig. 3b)).

Results and Discussion

Temperature Measurements

The results of the temperature measurements for different interlayer waiting periods and for the two wire speeds are visualized in Fig. 4. Remarkably, although twice as much material was deposited for the configuration with the higher wire speed, the measured temperatures for both configurations were very similar. Only a

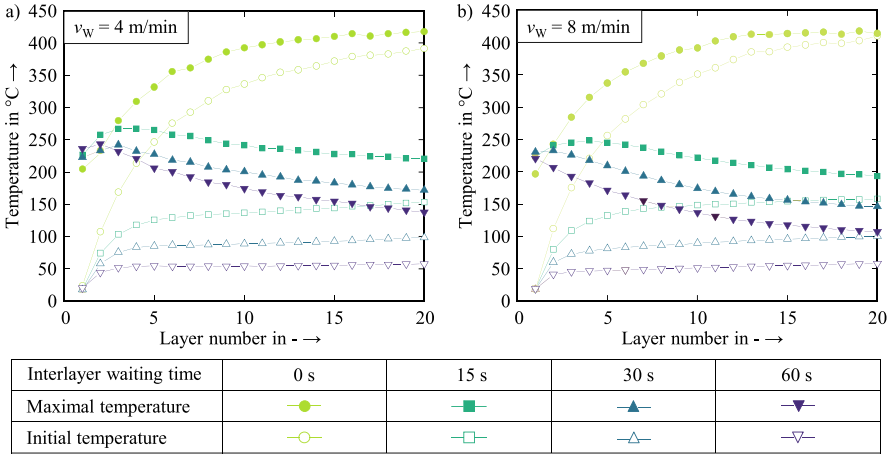

Fig. 4 Measured initial and maximal temperatures on the substrate resulting from different interlayer waiting times and for wire speeds of (**a**) 4 m/min and (**b**) 8 m/min

temperature difference of less than 30 K was noticeable in the recorded temperatures at the last layer. The high congruency can be attributed to the high thermal conductivity of aluminum alloys, which leads to a more homogenous temperature distribution in the part. For a t_{wait} of 0 s, both the initial and the maximal temperatures increased with each consecutive layer indicating a progressive heat accumulation in the part until reaching a plateau close to 400 °C. The heat accumulation in the part was drastically reduced by any of the implemented interlayer waiting periods, as the reached maximal temperatures were less than 270 °C. The maximal temperatures were measured after the first layers and decreased for consecutive layers because of the increasing distance between the location of the measurement and the process zone. For the interlayer waiting periods of 15 s, 30 s, and 60 s, the initial temperatures gradually increased until reaching plateaus approximately at 150 °C, 100 °C, and 60 °C. The results indicate that different initial temperatures can be deliberately set by implementing interlayer waiting periods. Notably, the initial temperatures can be interpreted as the temperature of a preheated substrate, strongly influencing the thermal conditions during the process. Thus, by selecting different interlayer temperatures, the thermal conditions, such as temperature gradients and cooling rates, can be altered.

Height and Width Measurements

In Fig. 5, the results of the width measurements are displayed including the respective standard deviations. Similar results were obtained for both wire speeds. A trend toward smaller widths for a higher T_{ini} was observable. However, the width at the bottom section remained almost constant. This can be explained by the fact, that the geometry of the initial layers was fully formed after their deposition. Any additional layer only had a thermal influence on the previous layers and did not affect their width. The width increase toward the upper region was especially noticeable in the part produced without any t_{wait} as this configuration led to the highest heat accumulation in the part. The heat accumulation led to a wider melt pool, which resulted in wider beads. The width differences between the top and bottom sections of up to 2 mm for the sample produced with $v_W = 8$ m/min and up to 1.5 mm for $v_W = 4$ m/min were reduced to 0.6 mm by implementing $t_{wait} = 15$ s and reached

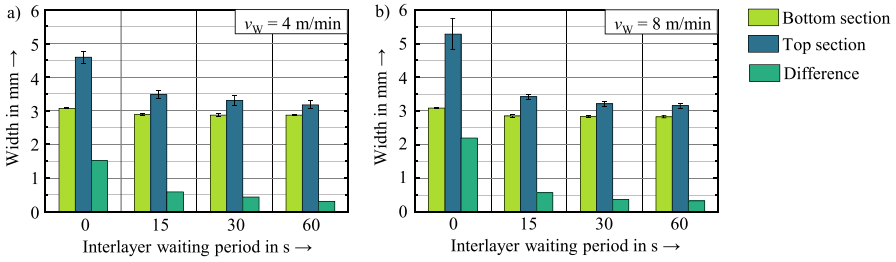

Fig. 5 Measured widths at the bottom and the top sections of the part as well as the width differences for wire speeds of (**a**) 4 m/min and (**b**) 8 m/min

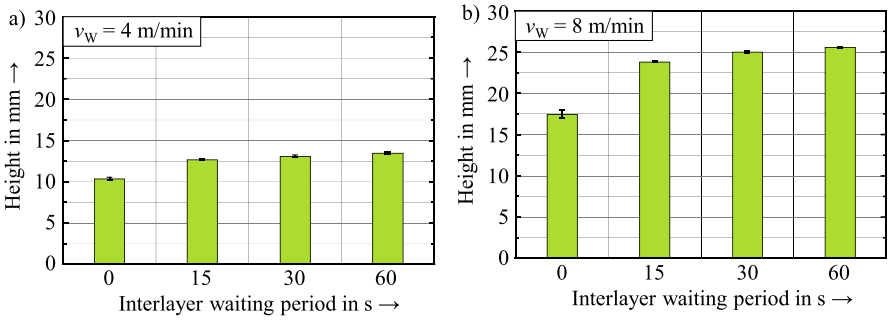

Fig. 6 Measured height of the parts for wire speeds of (**a**) 4 m/min and (**b**) 8 m/min

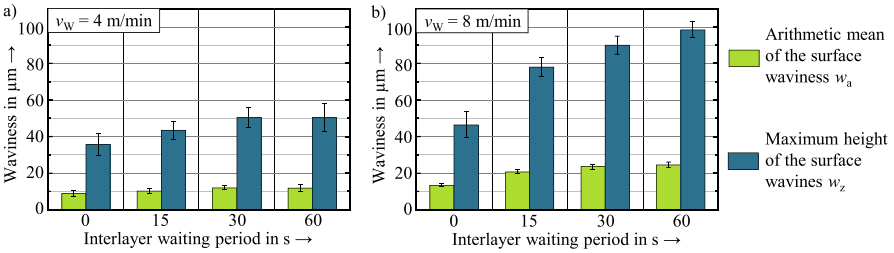

Fig. 7 Measured arithmetic mean and maximal height of the surface waviness of the parts for wire speeds of (**a**) 4 m/min and (**b**) 8 m/min

0.3 mm for t_{wait} = 60 s. Thus, more uniform wall widths were achieved for longer waiting periods.

Similar results were obtained for the height measurements displayed in Fig. 6. The increment of t_{wait} from 0 to 15 s had the largest impact and resulted in a height increment of 2.5 mm of the samples produced using v_W = 4 m/min and a height increment of 6 mm for the samples produced using v_W = 8 m/min. Further increasing t_{wait} had only a marginal effect on the height of the produced parts. These observations can be correlated to the width measurements. The heat accumulation in the parts led to wider beads at the top but with less height due to volume constancy. Contrary to the results for the width measurements, the height of the part strongly depended on the wire speed. By doubling v_W, also the height of the parts was doubled. This strong correlation resulted naturally since higher wire speeds mainly lead to higher beads, as analyzed in detail in the literature [40].

Waviness Measurements

Figure 7 shows the results of the waviness measurements. The waviness values obtained for a velocity of 8 m/min are approximately twice as high as those for 4 m/min. Still, the diagrams for both wire speeds show the same trend of a higher waviness for longer interlayer waiting periods. For v_W = 4 m/min, a maximal w_a = 12 µm

and a maximal w_z = 50 µm resulted, while for v_w = 8 m/min the measured maximal values were w_a = 23 µm and w_z = 99 µm. As shown in Fig. 4, shorter interlayer waiting periods resulted in higher interlayer temperatures. It can be assumed that the higher interlayer temperatures led to an increased remelting of the previous layers, thus progressively blurring the narrow sections between the layers. In contrast, less of the previous layer was remelted if the new layer was deposited on a colder layer, resulting in a pronounced narrow section between the layers. The higher deposition rate additionally increased the waviness since a more convex cross-sectional shape of each bead can be expected as more material is applied per layer.

Hardness Measurements

In Fig. 8, the results of the hardness measurements are displayed. It is noteworthy that for the parts that were produced without an interlayer waiting period, the hardness increased almost linearly from 70 $HV_{0.05}$ at the bottom section to 90 $HV_{0.05}$ at the top section. As reported in various literature sources, the hardness strongly correlates with the cooling rates [32]. Shortly before the process was stopped, it can be assumed that due to the high heat conductivity of aluminum alloys, the temperature at all layers of the part was fairly similar. This is also shown in Fig. 4, where the maximal measured temperatures for all layers only changed by approximately 50 and 100 K depending on the chosen t_{wait}. After the process was stopped, the layers that presumably cooled down the fastest were the ones at the top because of the rapid convective and radiant heat transfer facilitated by the high surface-to-volume ratio of the thin wall. The heat transmission toward the substrate in the case of t_{wait} = 0 s was not effective as the temperature of the substrate was around 400 °C (see Fig. 4). Therefore, the bottom section of the part cooled down the slowest, leaving more time for precipitation processes and, thus a lower hardness. With the implementation of interlayer waiting periods, the hardness distribution changed. In this case, the highest hardness values of 100 $HV_{0,05}$ resulted at the top and the bottom section of the part, while the center section of the wall featured a hardness of 90 $HV_{0,05}$. Similar hardness distribution, with the hardest sections located at the top and bottom, have been observed in previous studies using aluminum alloys [42]. The high hardness at the bottom of the part in these cases could have resulted in

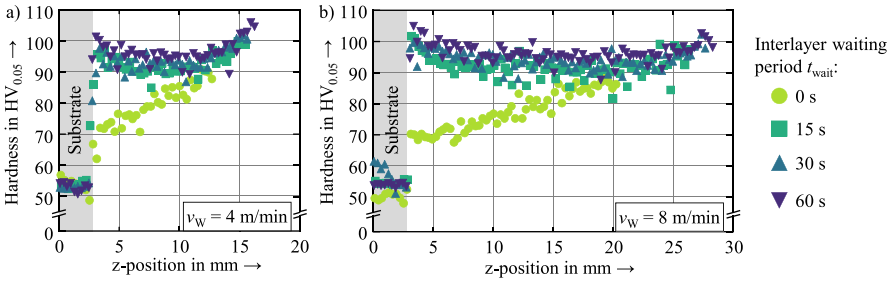

Fig. 8 Measured hardness of the parts resulting from different interlayer waiting times and for wire speeds of (**a**) 4 m/min and (**b**) 8 m/min

a faster cooling rate enabled by the lower initial temperature of the substrate. The relatively low temperature of the substrate of less than 150 °C allowed the heat to dissipate quickly, thus leaving less time for precipitation processes, resulting in a higher hardness.

As depicted in Fig. 9, the averaged hardness increased slightly with increasing interlayer waiting periods. The highest hardness increase from around 80 $HV_{0,05}$ to over 90 $HV_{0,05}$ resulted for the increment from an interlayer waiting period of 0 to 15 s. These hardness values are in accordance with works from the literature [20]. Longer waiting periods further increased the average hardness, however, the effect was less pronounced. The hardness increments were mainly attributed to the lower initial temperatures for each layer, thus resulting in higher cooling rates. Remarkably, the hardness values of both parts produced with different wire speeds were almost the same. Again, this can be explained by the high thermal conductivity of aluminum alloys, which led to similar thermal conditions despite the height difference of the parts.

Conclusions

In this work, the usage of DED-LB with wire feed was investigated for the rapid manufacturing or modification of aluminum alloy parts, with a specific focus on the geometrical features and the mechanical properties. Experiments were conducted using two significantly different wire speeds to emphasize the impact of the deposition rate on the outcome. Additionally, the effects of four different interlayer waiting periods on the part were examined. The following conclusions can be drawn based on the results:

- It was observed that the interlayer waiting periods were remarkably effective in preventing an overheating of the part. Implementing an interlayer waiting period of 15 s already hindered the progressive increase of the maximal temperature per layer measured on the substrate. By preventing overheating, the parts featured a more regular geometry and a higher hardness.

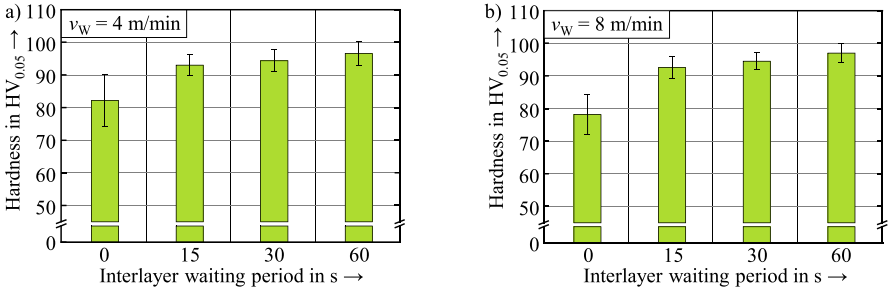

Fig. 9 Measured average hardness of the additive section of the parts resulting form different interlayer waiting times and for wire speeds of (**a**) 4 m/min and (**b**) 8 m/min

- Under the condition that overheating was prevented via interlayer waiting periods, the deposition rate predominantly affected the height and the surface quality of the part but not its width. The increased additional material fed per unit length mainly led to a higher part with a more wavy surface at the sides. On the contrary, low deposition rates resulted in a lower build-up but with a less wavy surface.
- Due to the high heat conductivity of aluminum alloys, the deposition rate had only a minor impact on the resulting temperature field. Consequently, comparable hardness values were obtained for both tested deposition rates. It was observed that the averaged hardness increased for longer interlayer waiting periods, likely because of the cooler substrate that led to faster cooling rates.

The results underline the high customization potential of the DED-LB-W process. It is possible to optimize the process for either a rapid build-up or a high surface quality through the process design. Moreover, the process design enables fine-tuning mechanical properties, such as the hardness. Thus, in the future, highly customized lightweight parts can be produced with this process. However, further studies are needed. For example, tensile strength tests would be beneficial to further characterize the produced parts. Additionally, depending on the surface conditions, the required post-processing of the parts needs to be evaluated. Also, a better understanding of the hardening mechanisms could be achieved by a more in-depth analysis of the evolution of the temperature field in the part. Thermal simulations would be an excellent tool for this purpose.

Author Contributions Conceptualization, A.Z.; methodology, A.Z., C. B.; validation, A.Z.; formal analysis, A.Z. and B.C.; investigation, A.Z. and M.C.; resources, M.F.Z.; data curation, A.Z. and M.C.; writing—original draft preparation, A.Z.; writing—review and editing, A.Z., C.B., and M.F.Z.; visualization, A.Z.; supervision, M.F.Z.; project administration, A.Z.; funding acquisition, A.Z. and M.F.Z.

Funding Open Access funding enabled and organized by Projekt DEAL. This study and the open access to the work was funded by the German Federal Ministry of Education and Research (BMBF) within the KORESIL project with the grant number 02P20Z002. We thank the Project Management Agency Karlsruhe (PTKA) for the supervision.

Data Availability The datasets generated during and/or analyzed during the current study are available from the corresponding author on reasonable request.

Declarations

Ethical Approval Not applicable.

Competing Interests The authors declare no competing interests.

References

1. Kamiya, G., Axsen, J., Crawford, C.: Modeling the GHG emissions intensity of plug-in electric vehicles using short-term and long-term perspectives. Transp. Res. Part. D. **69**, 209–223 (2019). https://doi.org/10.1016/j.trd.2019.01.027
2. Sanguesa, J.A., Torres-Sanz, V., Garrido, P., Martinez, F.J., Marquez-Barja, J.M.: A review on Electric vehicles: Technologies and challenges. Smart Cities. **4**, 372–404 (2021). https://doi.org/10.3390/smartcities4010022
3. Robert Bosch GmbH: Automotive Handbook. John Wiley & Sons, Newark, United Kingdom (2022)
4. Weiss, M., Cloos, K.C., Helmers, E.: Energy efficiency trade-offs in small to large electric vehicles. Environ. Sci. Eur. **32**, 46 (2020). https://doi.org/10.1186/s12302-020-00307-8
5. Nicoletti, L., Romano, A., König, A., Köhler, P., Heinrich, M., Lienkamp, M.: An estimation of the Lightweight Potential of Battery Electric Vehicles. Energies. **14**, 4655 (2021). https://doi.org/10.3390/en14154655
6. Orme, M., Madera, I., Gschweitl, M., Ferrari, M.: Topology Optimization for Additive Manufacturing as an enabler for Light Weight Flight Hardware. Designs. **2**, 51 (2018). https://doi.org/10.3390/designs2040051
7. Bassoli, E., Defanti, S., Tognoli, E., Vincenzi, N., Esposti, D.: Design for Additive Manufacturing and for Machining in the Automotive Field. Appl. Sci. **11**, 7559 (2021). https://doi.org/10.3390/app11167559
8. Gutowski, T., Jiang, S., Cooper, D., Corman, G., Hausmann, M., Manson, J.-A., Schudeleit, T., Wegener, K., Sabelle, M., Ramos-Grez, J., Sekulic, D.P.: Note on the rate and energy efficiency limits for Additive Manufacturing. J. Ind. Ecol. **21**, 69–79 (2017). https://doi.org/10.1111/jiec.12664
9. Abioye, T.E., Folkes, J., Clare, A.T.: A parametric study of Inconel 625 wire laser deposition. J. Mater. Process. Technol. **213**, 2145–2151 (2013). https://doi.org/10.1016/j.jmatprotec.2013.06.007
10. Zapata, A., Benda, A., Spreitler, M., Zhao, X.F., Bernauer, C., Yoshioka, H., Zaeh, M.F.: A model-based approach to reduce kinematics-related overfill in robot-guided laser Directed Energy Deposition. CIRP J. Manuf. Sci. Technol. **45**, 200–209 (2023). https://doi.org/10.1016/j.cirpj.2023.06.014
11. Dass, A., Moridi, A.: State of the art in Directed Energy Deposition: From Additive Manufacturing to materials Design. Coatings. **9**, 418 (2019). https://doi.org/10.3390/coatings9070418
12. Syed, W.U.H., Li, L.: Effects of wire feeding direction and location in multiple layer diode laser direct metal deposition. Appl. Surf. Sci. **248**, 518–524 (2005). https://doi.org/10.1016/j.apsusc.2005.03.039
13. Shakhverdova, I., Nowotny, S., Thieme, S., Kubisch, F., Beyer, E., Leyens, C.: Coaxial Laser Wire Deposition. J. Phys. Conf. Ser. **1109**, 12026 (2018). https://doi.org/10.1088/1742-6596/1109/1/012026
14. Kelbassa, J., Biber, A., Wissenbach, K., Loosten, J.H., Gasser, A., Pütsch, O., Loosen, P., Schleifenbaum, J.: Influence of focal length on the laser metal deposition process with coaxial wire feeding. In: Proceedings SPIE, San Francisco, USA, 2–7 February (2019). https://doi.org/10.1117/12.2507799
15. Zapata, A., Zhao, X.F., Li, S., Bernauer, C., Zaeh, M.F.: Three-dimensional annular heat source for the thermal simulation of coaxial laser metal deposition with wire. J. Laser Appl. **35**, 12020 (2023). https://doi.org/10.2351/7.0000813
16. Govekar, E., Jeromen, A., Kuznetsov, A., Kotar, M., Kondo, M.: Annular laser beam based direct metal deposition. Procedia CIRP. **74**, 222–227 (2018). https://doi.org/10.1016/j.procir.2018.08.099
17. Herrmann, C., Dewulf, W., Hauschild, M., Kaluza, A., Kara, S., Skerlos, S.: Life cycle engineering of lightweight structures. CIRP Ann. **67**, 651–672 (2018). https://doi.org/10.1016/j.cirp.2018.05.008
18. Tisza, M., Czinege, I.: Comparative study of the application of steels and aluminium in lightweight production of automotive parts. Int. J. Lightweight Mater. Manuf. **1**, 229–238 (2018). https://doi.org/10.1016/j.ijlmm.2018.09.001

19. an Wang, Wang, H., Wu, Y., Wang, H.: 3D printing of aluminum alloys using laser powder deposition: A review. Int. J. Adv. Manuf. Technol. **116**, 1–37 (2021). https://doi.org/10.1007/s00170-021-07440-5
20. Gao, Y., Zhao, J., Zhao, Y., Wang, Z., Song, H., Gao, M.: Effect of processing parameters on solidification defects behavior of laser deposited AlSi10Mg alloy. Vacuum. **167**, 471–478 (2019). https://doi.org/10.1016/j.vacuum.2019.06.042
21. Chen, B., Yao, Y., Song, X., Tan, C., Cao, L., Feng, J.: Microstructure and mechanical properties of additive manufacturing AlSi10Mg alloy using direct metal deposition. Ferroelectrics. **523**, 153–166 (2018). https://doi.org/10.1080/00150193.2018.1392147
22. Zhou, L., Mehta, A., Schulz, E., McWilliams, B., Cho, K., Sohn, Y.: Microstructure, precipitates and hardness of selectively laser melted AlSi10Mg alloy before and after heat treatment. Mater. Charact. **143**, 5–17 (2018). https://doi.org/10.1016/j.matchar.2018.04.022
23. Girelli, L., Tocci, M., Gelfi, M., Pola, A.: Study of heat treatment parameters for additively manufactured AlSi10Mg in comparison with corresponding cast alloy. Mater. Sci. Eng. A. **739**, 317–328 (2019). https://doi.org/10.1016/j.msea.2018.10.026
24. Shakil, S.I., Hadadzadeh, A., Shalchi Amirkhiz, B., Pirgazi, H., Mohammadi, M., Haghshenas, M.: Additive manufactured versus cast AlSi10Mg alloy: Microstructure and micromechanics. Res. Mater. **10**, 100178 (2021). https://doi.org/10.1016/j.rinma.2021.100178
25. Kronthaler, M.R., Spengler, S., Zaeh, M.F.: Bifocal hybrid laser welding - Fillet welds of aluminium. In: International Congress on Applications of Lasers & Electro-Optics ICALEO®, Orlando, Florida, USA, 23–27 October (2011). https://doi.org/10.2351/1.5062299
26. Nahmany, M., Shribman, V., Levi, S., Ashkenazi, D., Stern, A.: On Additive Manufactured AlSi10Mg to wrought AA6060-T6: Characterisation of optimal- and high-energy magnetic pulse welding conditions. Metals. **10**, 1235 (2020). https://doi.org/10.3390/met10091235
27. Shribman, V., Nahmany, M., Levi, S., Atiya, O., Ashkenazi, D., Stern, A.: MP Welding of dissimilar materials: AM laser powder-bed fusion AlSi10Mg to wrought AA6060-T6. Prog Addit. Manuf. **5**, 171–181 (2020). https://doi.org/10.1007/s40964-019-00100-x
28. Piscopo, G., Iuliano, L.: Current research and industrial application of laser powder directed energy deposition. Int. J. Adv. Manuf. Technol. **119**, 6893–6917 (2022). https://doi.org/10.1007/s00170-021-08596-w
29. Hermann, F., Vogt, S., Göbel, M., Möller, M., Frey, K.: Laser metal deposition of AlSi10Mg with high build rates. Procedia CIRP. **111**, 210–213 (2022). https://doi.org/10.1016/j.procir.2022.08.050
30. Saboori, A., Aversa, A., Marchese, G., Biamino, S., Lombardi, M., Fino, P.: Application of Directed Energy deposition-based Additive Manufacturing in Repair. Appl. Sci. **9**, 3316 (2019). https://doi.org/10.3390/app9163316
31. Bruzzo, F., Medapati, M.P.R., Pullini, D., Ronco, F., Bertinetti, A., Tommasi, A., Riede, M., Lòpez, E., Brückner, F.: Sustainable laser metal deposition of aluminum alloys for the automotive industry. J. Laser Appl. **34**, 042004 (2022). https://doi.org/10.2351/7.0000741
32. Hagenlocher, C., O'Toole, P., Xu, W., Brandt, M., Easton, M., Molotnikov, A.: The Effect of Heat Accumulation on the local grain structure in Laser-Directed Energy Deposition of Aluminium. Metals. **12**, 1601 (2022). https://doi.org/10.3390/met12101601
33. Froend, M., Ventzke, V., Kashaev, N., Klusemann, B., Enz, J.: Thermal analysis of wire-based direct energy deposition of Al-Mg using different laser irradiances. Addit. Manuf. **29**, 100800 (2019). https://doi.org/10.1016/j.addma.2019.100800
34. Kiani, P., Dupuy, A.D., Ma, K., Schoenung, J.M.: Directed energy deposition of AlSi10Mg: Single track nonscalability and bulk properties. Mater. Des. **194**, 108847 (2020). https://doi.org/10.1016/j.matdes.2020.108847
35. Becker, D., Boley, S., Eisseler, R., Stehle, T., Möhring, H.-C., Onuseit, V., Hoßfeld, M., Graf, T.: Influence of a closed-loop controlled laser metal wire deposition process of S Al 5356 on the quality of manufactured parts before and after subsequent machining. Prod. Eng. Res. Dev. **15**, 489–507 (2021). https://doi.org/10.1007/s11740-021-01030-w
36. Möhring, H.-C., Becker, D., Eisseler, R., Stehle, T., Reeber, T.: Influence of the manufacturing parameters of an AlMg5 wire–based hybrid production process on quality and mechanical properties. Int. J. Adv. Manuf. Syst. **119**, 2445–2460 (2022). https://doi.org/10.1007/s00170-021-08106-y
37. Madarieta, M., Irazu, E., Garmendia, I., Flores, J., Soriano, C.: Geometrical study of 5356 aluminium alloy by means of a concentric wire laser metal deposition. Procedia CIRP. **113**, 361–366 (2022). https://doi.org/10.1016/j.procir.2022.09.143

38. Abuabiah, M., Mbodj, N.G., Shaqour, B., Herzallah, L., Juaidi, A., Abdallah, R., Plapper, P.: Advancements in laser wire-feed metal Additive Manufacturing: A brief review. Materials. **16**, 2030 (2023). https://doi.org/10.3390/ma16052030
39. Bernauer, C., Zapata, A., Zaeh, M.F.: Toward defect-free components in laser metal deposition with coaxial wire feeding through closed-loop control of the melt pool temperature. J. Laser Appl. **34**, 042044 (2022). https://doi.org/10.2351/7.0000773
40. Zapata, A., Bernauer, C., Stadter, C., Kolb, C.G., Zaeh, M.F.: Investigation on the cause-Effect relationships between the process parameters and the resulting geometric properties for Wire-based Coaxial Laser Metal Deposition. Metals. **12**, 455 (2022). https://doi.org/10.3390/met12030455
41. Baier, D., Wolf, F., Weckenmann, T., Lehmann, M., Zaeh, M.F.: Thermal process monitoring and control for a near-net-shape Wire and Arc Additive Manufacturing. Prod. Eng. Res. Dev. **16**, 811–822 (2022). https://doi.org/10.1007/s11740-022-01138-7
42. Demir, A.G.: Micro laser metal wire deposition for additive manufacturing of thin-walled structures. Opt. Lasers Eng. **100**, 9–17 (2018). https://doi.org/10.1016/j.optlaseng.2017.07.003